JACS
JOURNAL OF THE AMERICAN CHEMICAL SOCIETY
pubs.acs.org/JACS
Article

# Unraveling the Complexity of Supramolecular Copolymerization Dictated by Triazine−Benzene Interactions

Hao Su, Stef A. H. Jansen, Tobias Schnitzer, Elisabeth Weyandt, Andreas T. Rösch, Jie Liu, Ghislaine Vantomme, and E. W. Meijer*

Cite This: J. Am. Chem. Soc. 2021, 143, 17128−17135
Read Online
ACCESS | Metrics & More | Article Recommendations | Supporting Information

**ABSTRACT:** Supramolecular copolymers formed by the noncovalent synthesis of multiple components expand the complexity of functional molecular systems. However, varying the composition and microstructure of copolymers through tuning the interactions between building blocks remains a challenge. Here, we report a remarkable discovery of the temperature-dependent supramolecular copolymerization of the two chiral monomers 4,4′,4″-(1,3,5-triazine-2,4,6-triyl)tribenzamide (***S*-T**) and 4,4′,4″-(benzene-1,3,5-triyl)tribenzamide (***S*-B**). We first demonstrate in the homopolymerization of the two individual monomers that a subtle change from the central triazine to benzene in the chemical structure of the monomers significantly affects the properties of the resulting homopolymers in solution. Homopolymers formed by ***S*-T** exhibit enhanced stability in comparison to ***S*-B**. More importantly, through a combination of spectroscopic analysis and theoretical simulation, we reveal the complex process of copolymerization: ***S*-T** aggregates into homopolymers at elevated temperature, and upon slow cooling ***S*-B** gradually intercalates into the copolymers, to finally give copolymers with almost 80% alternating bonds at 10 °C. The formation of the predominantly alternating copolymers is plausibly contributed by preferred heterointeractions between triazine and benzene cores in ***S*-T** and ***S*-B**, respectively, at lower temperatures. Overall, this work unravels the complexity of a supramolecular copolymerization process where an intermediate heterointeraction (higher than one homointeraction and lower than the other homointeraction) presents and proposes a general method to elucidate the microstructures of copolymers responsive to temperature changes.

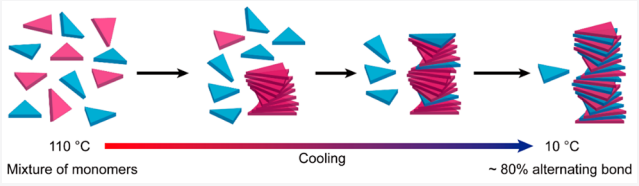


## INTRODUCTION

The potential applications of supramolecular polymers in pharmaceuticals,[1−3] nanoelectronics,[4,5] and catalysis[6−8] have motivated growing interest in further exploring the field. With the aim to create competitive functional materials, a big step forward is to integrate different monomers into supramolecular copolymers through noncovalent heterointeractions.[9] Although copolymerization offers a promising strategy to make multifunctional systems with emerging properties, constructing precisely controlled multicomponent copolymers is challenging, as a fundamental understanding of these complex systems has not been fully developed. Typically, in a two-component system consisting of monomers **A** and **B**, depending on the interplay between the monomers, the microstructures of the copolymers can vary from one extreme to another: that is, total self-sorting to completely alternating.[10] The degree of copolymerization can be determined by the reactivity ratio $R$,[10] defined as the ratio of Gibbs free energy change of the homoaggregation ($\Delta G_{A\text{-}A} + \Delta G_{B\text{-}B}$) to the Gibbs free energy change of the heteroaggregation ($\Delta G_{A\text{-}B} + \Delta G_{B\text{-}A}$) of the whole system. If $R > 1$, homointeractions are more favored; if $R < 1$, heterointeractions are favored. In the former case of self-sorted homopolymers where $R$ approaches infinity, the monomers can distinguish between self and nonself in the system.[11,12] In the latter case of alternating copolymers where $R < 1$, the introduction of strong heterointeractions, such as charge transfer interactions and electrostatic interactions, between monomers gives perfectly alternating supramolecular copolymers.[13−16] However, most cases are often not under these extreme, yet simple, conditions.[10,17−22] Therefore, it is important to unravel the complexity and predict the microstructures of supramolecular copolymer systems.

Here, we present an example of a two-component supramolecular copolymerization using a combination of spectroscopic analysis and theoretical simulation, where the microstructures are highly dependent on the temperatures. Figure 1A shows the design of the two chiral monomers 4,4′,4″-(1,3,5-triazine-2,4,6-triyl)tribenzamide (**S-T**) and 4,4′,4″-(benzene-1,3,5-triyl)tribenzamide (***S*-B**), which are structurally similar but have a triazine unit and a benzene unit in the center of the cores, respectively. The $C_3$-symmetric

Received: July 23, 2021
Published: October 6, 2021





https://doi.org/10.1021/jacs.1c07690
J. Am. Chem. Soc. 2021, 143, 17128−17135

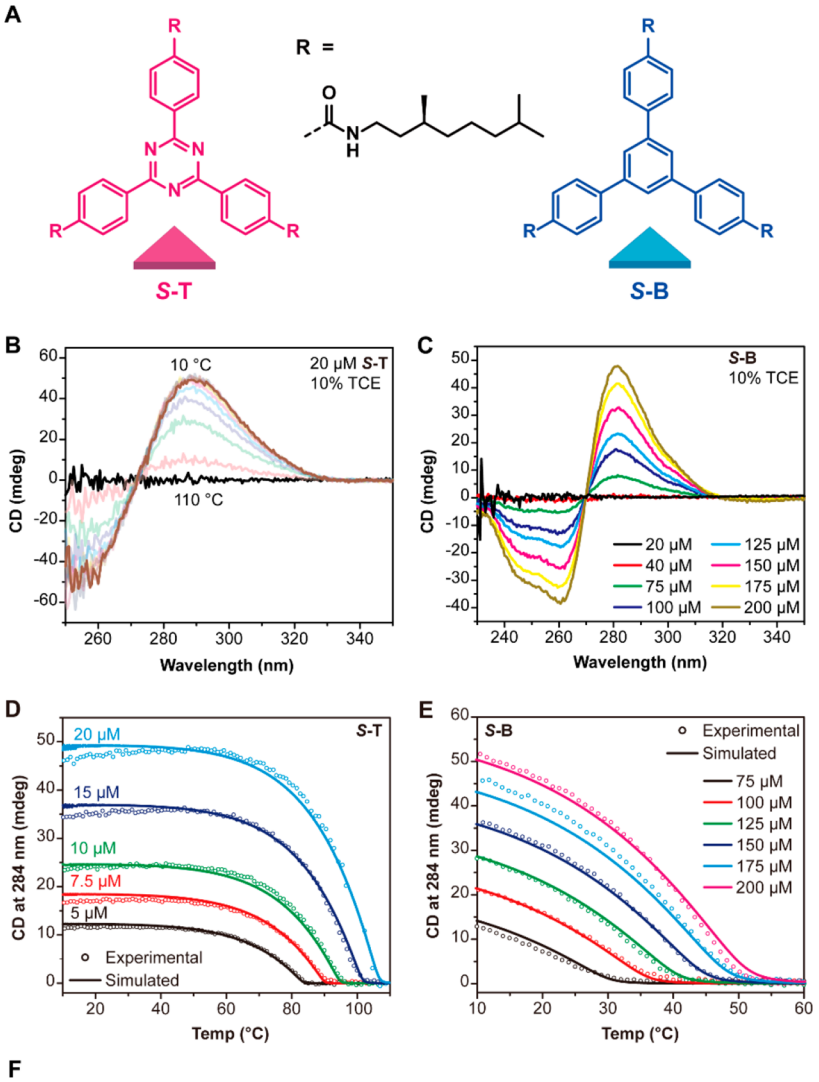


F

| | $\Delta H_e$ (kJ·mol$^{-1}$) | $\Delta S$ (kJ·mol$^{-1}$·K$^{-1}$) | $NP^a$ (kJ·mol$^{-1}$) | $\sigma^b$ (--) |
|---|---|---|---|---|
| **S-T** | -67.7 | -0.089 | 30.2 | $4.1 \cdot 10^{-6}$ |
| **S-B** | -38.7 | -0.049 | 18.7 | $4.7 \cdot 10^{-4}$ |

**Figure 1.** Supramolecular homopolymerization of ***S*-T** and ***S*-B** in decalin with 10% TCE. (A) Chemical structures and cartoons of ***S*-T** and ***S*-B** monomers. (B) Temperature interval CD spectra of ***S*-T** obtained via slow cooling from 110 to 10 °C at 10 °C intervals. (C) CD spectra of ***S*-B** at various concentrations at 20 °C. (D, E) Experimental (circles) and simulated (lines, using a mass-balance model) CD cooling curves of the supramolecular homopolymerization of (D) ***S*-T** and (E) ***S*-B** at various concentrations. (F) Table of optimized thermodynamic parameters for homopolymerization of ***S*-T** and ***S*-B**, determined by fitting the model for cooperative polymerization to the experimental data. Legend: (a) *NP* indicates the enthalpic nucleation penalty; (b) The cooperativity parameter specified is calculated at 20 °C. Conditions: cooling rate of all the measurements: ,1 °C/min; optical path length, 1 cm for concentrations ≤40 $\mu$M and 0.1 cm for concentrations >40 $\mu$M.

shape, resembling that of benzene-1,3,5-tricarboxamide (BTA) derivatives, is known to facilitate dynamic supramolecular assemblies via 3-fold H-bonding interactions.[23] The electron-poor surface of triazine and the electron-rich surface of benzene could provide specific intermolecular interactions between the monomers.[24] In this system, the homointeraction between ***S*-T** monomers is strong, the heterointeraction between ***S*-T** and ***S*-B** monomers is intermediate, and the homointeraction between ***S*-B** monomers is very weak. The strong **T−T** interaction makes monomer ***S*-T** aggregate into homopolymers even at elevated temperatures, while ***S*-B** does not polymerize on its own under the same conditions. The coexistence of strong and weak homointeractions and intermediate heterointeractions makes the system very complicated. In addition, these interactions are responsive to temperature; as a result the values of the reactivity ratio *R* are also temperature-dependent. Therefore, it is important to investigate this complex supramolecular copolymerization system, where the strengths of heterointeractions fall between those of two homointeractions, as well as to study the microstructures of the polymers at various temperatures. We found that, in the copolymerization process, ***S*-T** aggregates into homopolymers at high temperature and ***S*-B** gradually intercalates into the copolymers upon cooling. Importantly, the corresponding *R* value of the whole system decreases from 1.07 at 110 °C to 0.91 at 10 °C, which is in line with the evolution


https://doi.org/10.1021/jacs.1c07690
J. Am. Chem. Soc. 2021, 143, 17128−17135

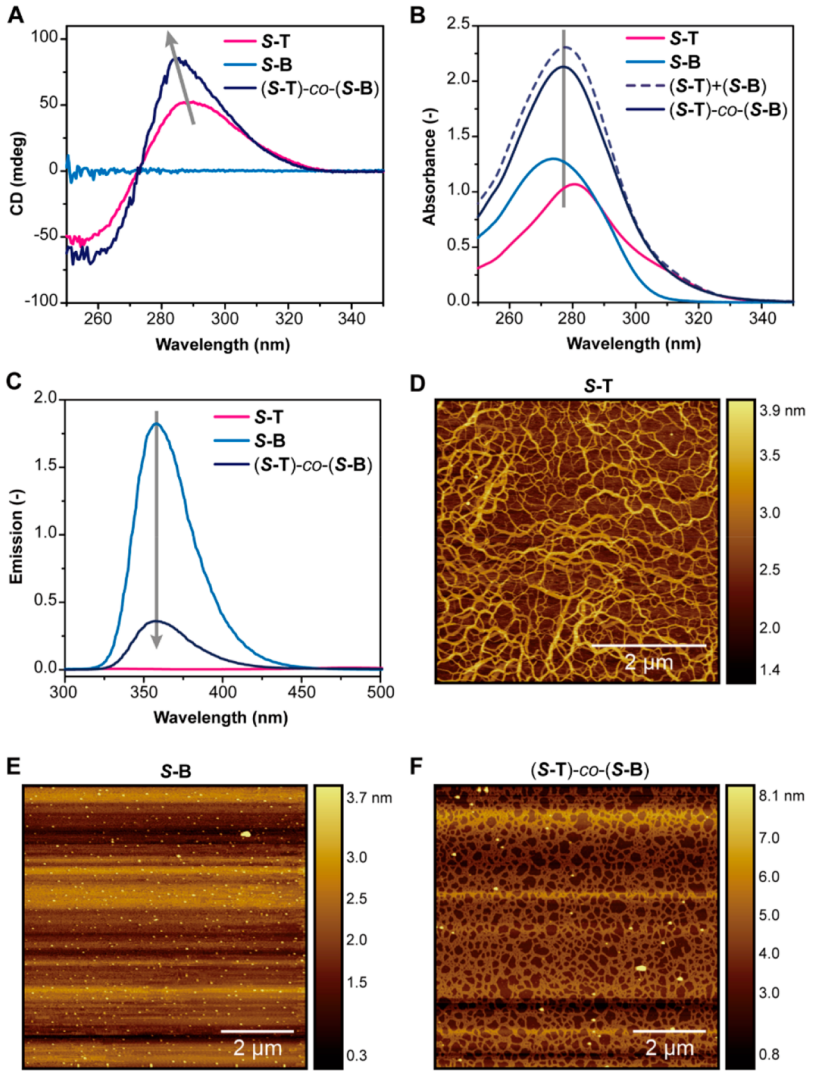


**Figure 2.** Supramolecular copolymerization of ***S*-T** and ***S*-B** in decalin with 10% TCE. (A) CD, (B) UV−vis, and (C) emission spectra ($\lambda_{exc}$ = 284 nm) of ***S*-T**, ***S*-B**, and (***S*-T**)-*co*-(***S*-B**) in solution at 20 °C. Conditions: solvent, decalin with 10% TCE; concentrations, ***S*-T** (20 $\mu$M), ***S*-B** (20 $\mu$M), and (***S*-T**)-*co*-(***S*-B**) (20 $\mu$M + 20 $\mu$M); optical path length, 1 cm. AFM images of (D) ***S*-T** (20 $\mu$M), (E) ***S*-B** (20 $\mu$M), and (F) (***S*-T**)-*co*-(***S*-B**) (20 $\mu$M + 20 $\mu$M). AFM samples were prepared via drop-casting sample solutions onto mica sheets.

of microstructures from homopolymers to predominantly alternating copolymers.

## RESULTS AND DISCUSSION

The formation of supramolecular polymers was investigated by dissolving the monomers in decalin with 10% of the chlorinated solvent 1,1,2,2-tetrachloroethane (TCE). The use of decalin with 10% TCE as the solvent is to ensure that the supramolecular polymers are in a thermodynamically stable state, since ***S*-T** supramolecular polymers (20 $\mu$M) cannot completely dissociate into a monomeric state in pure decalin or decalin with 5% TCE even at a temperature of 110 °C (Figure S1; see section S4 in the Supporting Information for more detailed studies), which is the temperature limit of our instrumentation. The supramolecular polymerization process of ***S*-T** (20 $\mu$M) in decalin with 10% TCE was analyzed by temperature-interval CD (Figure 1B) and UV−vis (Figure S2) spectroscopic measurements by slow cooling of the solutions from 110 to 10 °C at a rate of 1 °C/min. We observed an increase in the CD signal with a maximum positive absorption at 289 nm and a shift in the UV−vis absorption bands from 286 nm to a lower wavelength of 282 nm, indicating the occurrence of the supramolecular polymerization of ***S*-T** (20 $\mu$M in decalin with 10% TCE) (Figure 1B and Figure S2) upon cooling. However, for ***S*-B**, no CD signals were observed at concentrations of 20 and 40 $\mu$M at 20 °C (Figure 1C), suggesting that no supramolecular polymers were formed. Higher concentrations are needed to induce the aggregation of monomers (Figure 1C). Altogether, these results suggest that ***S*-T** monomers have stronger tendency to aggregate into supramolecular homopolymers in comparison with ***S*-B** monomers at the same concentration and temperature.

Monitoring the CD values at the wavelength of 284 nm upon cooling generated nonsigmoidal curves for both molecules (Figure 1D,E). The sharp transitions around the temperature of elongation ($T_e$) suggest that the homopolymerization of both ***S*-T** and ***S*-B** follows a cooperative nucleation−elongation mechanism.[25] A thermodynamic mass-balance model (see the Supporting Information for details) for cooperative polymerizations, as reported by Zhao and Moore,[26] was fitted to the experimental variable-temperature (VT)-CD curves at various concentrations (Figure 1D,E), and


https://doi.org/10.1021/jacs.1c07690
J. Am. Chem. Soc. 2021, 143, 17128−17135

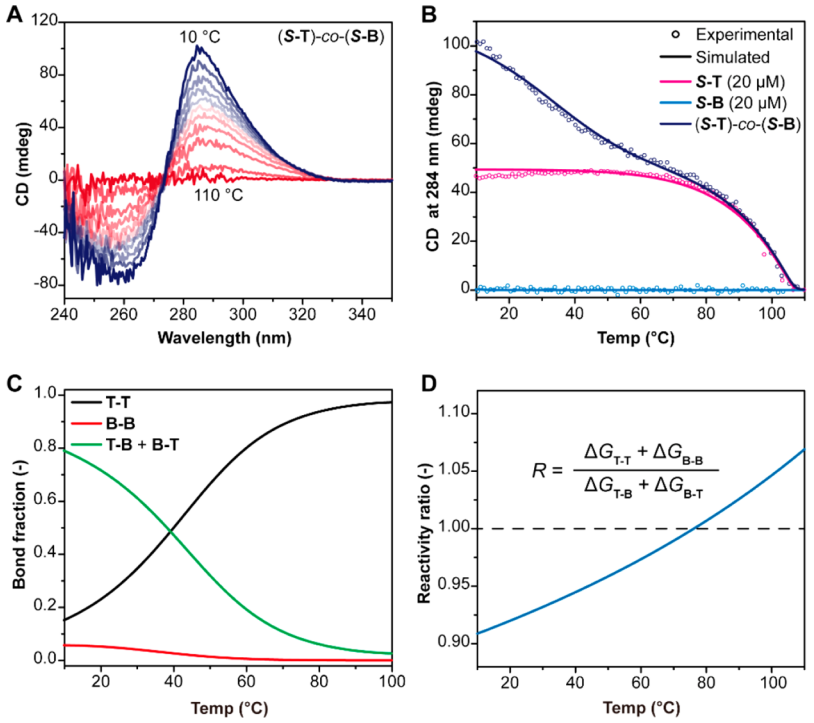


**Figure 3.** Experimental and simulated results indicate predominant alternating assembly in supramolecular copolymer (***S*-T**)-*co*-(***S*-B**) at low temperature. (A) Temperature interval CD spectra of (***S*-T**)-*co*-(***S*-B**) obtained via slow cooling from 110 to 10 °C with 10 °C intervals. (B) Experimental (circles) and simulated (lines) CD cooling curves of the supramolecular polymerization of ***S*-T**, ***S*-B**, and (***S*-T**)-*co*-(***S*-B**). Conditions: optical path length, 1 cm; concentration, 20 $\mu$M for ***S*-T** and 20 $\mu$M for ***S*-B**; solvent, decalin with 10% TCE; cooling rate of measurements, 1 °C/min. (C) Calculated fractions of bonds in the solution. Monomer **T** represents ***S*-T**, and monomer **B** represents ***S*-B**. (**D**) Temperature-dependent reactivity ratio $R$ calculated by the ratio of Gibbs free energy change of the homoaggregation to the heteroaggregation. Plots in (C) and (D) were generated via simulations based on experimental data using the mass-balance copolymerization model.

the optimized thermodynamic parameters for ***S*-T** and ***S*-B** are summarized in Figure 1F. The obtained enthalpy and entropy values ($\Delta H_{T\text{-}T}$ = −67.7 kJ mol$^{-1}$, $\Delta S_{T\text{-}T}$ = −0.089 kJ mol$^{-1}$ K$^{-1}$, $\Delta H_{B\text{-}B}$ = −38.7 kJ mol$^{-1}$, and $\Delta S_{B\text{-}B}$ = −0.049 kJ mol$^{-1}$ K$^{-1}$) reflect that the assembly of ***S*-T** is more favorable than that of ***S*-B**, and as indicated by the nucleation penalty ($NP_{S\text{-}T}$ = 30.2 kJ mol$^{-1}$ and $NP_{S\text{-}B}$ = 18.7 kJ mol$^{-1}$), ***S*-T** shows much higher cooperativity ($\sigma_{S\text{-}T}$ = 4.1 × 10$^{-6}$ at 20 °C) in comparison with ***S*-B** ($\sigma_{S\text{-}B}$ = 4.7 × 10$^{-4}$ at 20 °C). Since the only difference between ***S*-T** and ***S*-B** monomers is the central triazine and benzene, we set out to investigate how the cores can affect the intermolecular interactions by computational studies (see section S6 in the Supporting Information). Therefore, we carried out density functional theory (DFT) calculations on monomers and homodimers of ***S*-T** and ***S*-B**. The differences in stability of the aggregates can be explained by a conformational analysis of dihedral angles of the central triazine or benzene ring with the peripheral phenyl rings (Figure S3). We observed an almost flat conformation for the ***S*-T** monomer (∼179°), while the dihedral angles in ***S*-B** are around 139° (Figure S3), which are similar to previously reported values.[27] Also, the calculated relative total energy for the ***S*-T** homodimer is lower than that for the ***S*-B** homodimer (Table S2). We reason that the higher planarity of ***S*-T** enables better intermolecular amide−amide bond formations in comparison to ***S*-B**, and therefore supramolecular ***S*-T** polymers are more stable than ***S*-B** polymers under same conditions.

Given our understanding on homopolymerizations, we next studied the supramolecular copolymerization of ***S*-T** and ***S*-B** in decalin with 10% TCE. First, solutions at a total concentration of 40 $\mu$M (20 $\mu$M ***S*-T** + 20 $\mu$M ***S*-B**) were prepared by mixing equal volumes of the stock solutions (40 $\mu$M). After heating to 110 °C and slow cooling to 20 °C, we measured the CD, UV−vis, and fluorescence spectra of the solution. The CD intensity of the mixture significantly increased from 52 to 81 mdeg at 289 nm, and the maximum shifted from 289 to 284 nm in comparison with ***S*-T** homopolymers alone, while a pure ***S*-B** solution showed no CD signal at 20 $\mu$M (Figure 2A). The UV−vis absorbance of the mixture is lower than the linear sum of the absorbance of the two individual solutions at the same wavelength ($\lambda$ = 277 nm), indicating that the difference in intensity is cause by heterointeractions (Figure 2B). Furthermore, we observed quenching of fluorescence in the ***S*-T** and ***S*-B** mixture in comparison with ***S*-B** alone (Figure 2C), while the emission of ***S*-T** homopolymers is negligible due to self-quenching of ***S*-T** monomers on assembly. Our findings strongly indicate that ***S*-T** and ***S*-B** can copolymerize into supramolecular copolymers even though ***S*-B** cannot polymerize by itself under these conditions. This conclusion was further supported by atomic force microscopy (AFM) measurements. Supramolecular fibers were observed for ***S*-T** homopolymers (Figure 2D), and irregular spherical objects were observed for ***S*-B** (Figure 2E). Upon mixing of the two monomers, fibers were observed (Figure 2F), suggesting the formation of the supramolecular copolymers.

To get more mechanistic insight into the supramolecular copolymerization, we next performed variable-temperature CD measurements upon slow cooling of an equimolar monomer solution at a concentration of 40 $\mu$M (20 $\mu$M ***S*-T** + 20 $\mu$M ***S*-**


https://doi.org/10.1021/jacs.1c07690
J. Am. Chem. Soc. 2021, 143, 17128−17135

**Scheme 1. Cartoon Illustration of Supramolecular Copolymerization of (*S*-T)-*co*-(*S*-B) (20 $\mu$M + 20 $\mu$M)**[a]

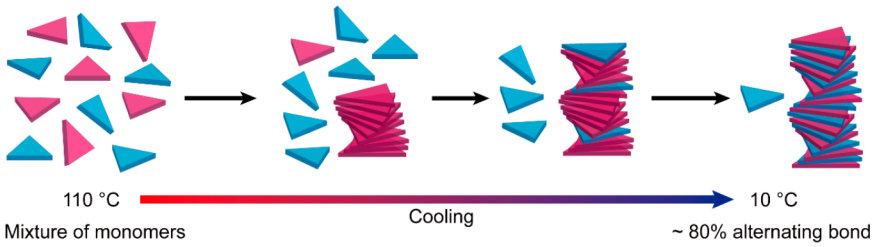


[a]Both ***S*-T** (purple) and ***S*-B** (blue) are monomerically dissolved at 110 °C. Upon continuous slow cooling, ***S*-T** monomers first aggregate into homopolymers with a few ***S*-B** monomers intercalating. A further decrease of temperature leads to more ***S*-B** monomers intercalating into the polymer via hetero-nteractions between ***S*-T** and ***S*-B** until finally almost 80% of the bonds are alternating at 10 °C.

**B**). As observed in Figure 3A, molecules are monomerically dissolved at 110 °C and start to polymerize upon cooling, as indicated by an increase in the CD intensity and a blue shift in the absorption maximum. Taking a closer look at the VT-CD cooling curves (Figure 3B), we surprisingly found that the cooling curve of the copolymers overlaps with that of ***S*-T** between 110 and 90 °C, and a further decrease of temperature results in a continuous increase of the CD signal, which exceeds the signal of ***S*-T**. No CD signal was observed for ***S*-B** alone, demonstrating that these monomers are molecularly dissolved in this concentration and temperature range. In addition, we performed a full cooling and heating cycle of the copolymer solution and found that the heating curve matches well with the cooling curve, showing that the copolymerization process is reversible, and the system is in thermodynamic equilibrium (Figure S4).

To further verify our above observation in supramolecular copolymerization of ***S*-T** and ***S*-B**, we performed the copolymerization of chiral ***S*-B** with an achiral version of triazine-based monomer ***a*-T** (see section 2.3 in the Supporting Information) at a total concentration of 40 $\mu$M (20 $\mu$M ***a*-T** + 20 $\mu$M ***S*-B**) (Figure S5). The experimental conditions were identical with those in the polymerization of (***S*-T**)-*co*-(***S*-B**), except for the substitution of ***S*-T** by ***a*-T**. The solution mixture showed a strong CD signal with an intensity maximum at around 284 nm, while no CD signals were observed for both ***a*-T** and ***S*-B** (Figure S5C). This observation suggested that chiral ***S*-B** copolymerized with ***a*-T** and dictated its helicity in the copolymers, which followed the "sergeants-and-soldiers" effect.[28] In addition, we recorded CD and UV−vis cooling curves at 284 nm of supramolecular copolymerization of (***a*-T**)-*co*-(***S*-B**) (20 $\mu$M + 20 $\mu$M). The decrease in UV−vis absorbance at 102 °C and the absence of a CD signal until 90 °C indicated the homopolymerization of ***a*-T** in this temperature range (Figure S5D). Further cooling led to an increase in the CD signal, which suggests that chiral ***S*-B** was incorporated into the copolymers. The results are consistent with the observations in the copolymerization of ***S*-T** and ***S*-B**.

By varying monomer ratios and concentrations in the copolymer solutions of (***S*-T**)-*co*-(***S*-B**), we experimentally measured various VT-CD cooling curves, which were fitted using a mass-balance model for copolymerizations as reported by ten Eikelder and co-workers (Figure 3B and Figure S6, see the Supporting Information for details).[29,30] In this model, it is assumed that homointeractions of monomers in the copolymers are identical with those in the homopolymers determined above (Figure 1F). The copolymerization model was fitted to CD cooling curves, in which the entropy and enthalpy of the interaction between the ***S*-T** and ***S*-B** monomers were used as fitting parameters. The resulting fit is shown in Figure S6, and the optimized thermodynamic parameters for the heterointeractions were determined as $\Delta H = -65.3$ kJ mol$^{-1}$ and $\Delta S = -0.120$ kJ mol$^{-1}$ K$^{-1}$ (Table S1). In comparison to the homointeractions (Figure 1F), the **T−B**/**B−T** heterointeractions (Table S1) seem to be more favorable than the **B−B** homointeraction but slightly less favorable than the **T−T** homointeraction. Our DFT calculations on heterodimers also confirmed that the calculated relative total energies for **T−B**/**B−T** heterodimers fall between those of **T−T** and **B−B** (Figure S3 and Table S2). In addition, we observe a relatively large value for $\Delta S$ ($-0.120$ kJ mol$^{-1}$ K$^{-1}$) (Table S1) for the interaction between ***S*-T** and ***S*-B**, making the heterointeraction less favorable at higher temperatures and more significant at lower temperatures in the simulations. This is in good agreement with the melting curves of the copolymers following the profile of ***S*-T** homopolymerization at high temperatures and showing copolymerization at temperatures below 90 °C.

The optimized thermodynamic parameters for the copolymerization of (***S*-T**)-*co*-(***S*-B**) (20 $\mu$M + 20 $\mu$M) (Figure 3B) were used to calculate the fractions of homobonds (**T−T** and **B−B**) and heterobonds (**T−B** and **B−T**) in the copolymers at variable temperatures (Figure 3C), as well as species in the solution mixture (Figure S7A), using the method reported by ten Eikelder and co-workers.[30] Above 90 °C, only **T−T** homobonds exist and there are no **B−B** homobonds or **T−B**/**B−T** heterobonds. Upon cooling below 90 °C, the fraction of **T−T** bonds decreases and the fraction of heterobonds (**T−B** + **B−T**) increases (Figure 3C). When the temperature goes further below 50 °C, the fraction of ***S*-B** in the copolymers significantly increases with the corresponding growing number of heterobonds (**T−B** + **B−T**). At 10 °C, all of the ***S*-T** monomers and over 90% of the total ***S*-B** monomers are in the copolymers. Importantly, the calculated fraction of free ***S*-B** monomer in solution is around 8% (Figure S7A), which is in line with free ***S*-B** (1.55 $\mu$M and 7.75% of total ***S*-B**) estimated experimentally via fluorescence measurements (Figure S8). In this regime, almost 80% of the bonds are alternating bonds (Figure 3C).

The observations above are intriguing, since we did not expect such a temperature-dependent change of microstructures in the polymers. In typical examples of alternating supramolecular polymers, each monomer itself is not able to homopolymerize on its own because of the stronger interactions between comonomers.[15] Therefore, in these cases, heteroaggregation is always much more favored than homoaggregation independent of the temperature regime.[10] In our case, the homopolymers of ***S*-T** form at high temperatures and ***S*-B** monomers incorporate into the copolymers as the


https://doi.org/10.1021/jacs.1c07690
J. Am. Chem. Soc. 2021, 143, 17128−17135

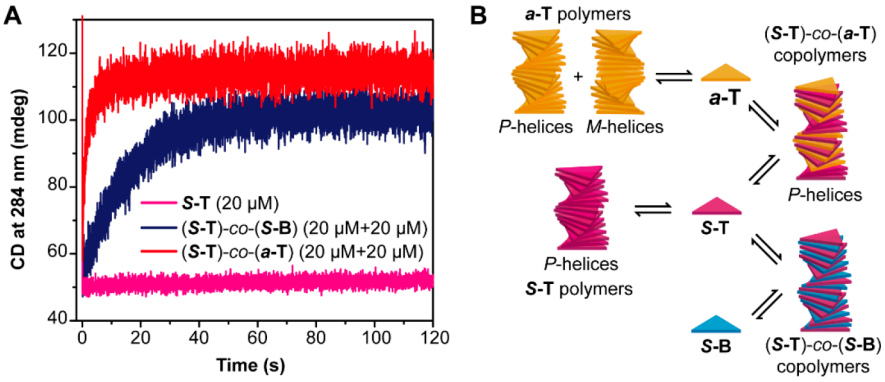


**Figure 4.** Copolymerization kinetics of ***S*-T** (20 $\mu$M), ***a*-T** (20 $\mu$M), and ***S*-B** (20 $\mu$M) at 10 °C. (A) In stopped-flow experiments, CD signals at 284 nm were monitored upon mixing ***S*-T** with ***a*-T** or ***S*-B** at equal volume to make the final concentration 20 $\mu$M for each monomer at 10 °C. The plots were averaged from three parallel measurements for each condition. (B) Schematic illustration of copolymerization process in dynamic systems.

temperature decreases. We speculate that the intercalation of ***S*-B** between two ***S*-T** molecules is a result of charge transfer interactions between triazine and benzene at low temperatures;[24] however, the interactions are not strong enough to make heterodimers at elevated temperature.

To probe the strength of the triazine−benzene interaction, we calculated the Gibbs free energy change of homodimers and heterodimers as a function of temperature (Figure S7B). The $\Delta G$ values of heterodimers decrease more quickly than those of homodimers upon cooling, indicating that the heterointeractions increase more quickly than homointeractions. From 110 to 10 °C, $\Delta G_{T\text{-}T}$ decreases from −33.8 to −42.7 kJ mol$^{-1}$, $\Delta G_{B\text{-}B}$ decreases from −19.9 to −24.8 kJ mol$^{-1}$, $\Delta G_{T\text{-}B}$ decreases from −19.3 to −31.4 kJ mol$^{-1}$, and $\Delta G_{B\text{-}T}$ decreases from −30.8 to −42.9 kJ mol$^{-1}$; therefore, the reactivity ratio $R$ of the whole system decreases from 1.07 at 110 °C to 0.91 at 10 °C (Figure 3D). If $R > 1$, homointeractions are more favored, and if $R < 1$, heterointeractions are favored; the smaller the $R$ value, the more alternating the structure. Our system presents a seminal case in which the $R$ value changes from above 1 to below 1 over temperature, making the supramolecular copolymerization process evolve from homopolymers to predominant alternating copolymers. More importantly, simulations using other ***S*-T** and ***S*-B** concentration combinations (Figure S9) support the proposed copolymerization process (Scheme 1) and provide the possibility of tuning the compositions of the copolymers.

Finally, we investigated the copolymerization kinetics by stopped-flow experiments, which helps to understand how ***S*-B** incorporates into the copolymers. Stock solutions of monomers were prepared at a concentration of 40 $\mu$M in decalin with 10% TCE. CD signals at 284 nm were monitored upon mixing ***S*-T**, ***a*-T** (achiral triazine-based monomer; see section 2.3 in the Supporting Information), or ***S*-B** in equal volumes to make the final concentration 20 $\mu$M for each monomer at 10 °C (Figure 4A). A 40 $\mu$M ***S*-T** solution was also mixed with an equal volume of solvent (decalin with 10% TCE) to give a 20 $\mu$M ***S*-T** solution as a control (Figure 4A, pink curve). The copolymerization of chiral ***S*-T** and achiral ***a*-T** monomers is a "sergeants-and-soldiers" experiment,[28] where the chiral ***S*-T** (sergeants) dictates the helicity to achiral ***a*-T** (soldiers) in the copolymers. We observe full expression of chirality amplification within 20 s (Figure 4A, red curve), showing that ***S*-T** polymers are not kinetically trapped and the whole system is highly dynamic. Also, the copolymerization of ***S*-T** and ***S*-B** approaches equilibrium within 60 s (Figure 4A, navy curve). The continuous increase in CD signal suggests that ***S*-B** monomers quickly incorporate into the copolymers. Since ***S*-T** homopolymers are very dynamic, we reason that ***S*-B** monomers may not directly chip into the preformed ***S*-T** homopolymeric stacks in the copolymerization. Although we sometimes use the word "*intercalation*" to describe the process, it is more about indicating that, in the equilibrated copolymers, ***S*-B** monomers intercalate between ***S*-T** monomers. We propose that the copolymerization of ***S*-T** and ***S*-B** is mostly caused by the nucleation of ***S*-T** and ***S*-B** monomers/clusters in the solution followed by continuous elongation (Figure 4B). The fast dynamicity of the system provides the possibility for quick exchange among the homopolymers, the monomers and the copolymers in solution, therefore enabling a real-time reconstruction of copolymer compositions.

## CONCLUSIONS

Here, we reported the analysis of a complex supramolecular copolymerization by combining experimental data and a theoretical simulation, where a prediction of the copolymer composition is achieved. In the copolymerization process, ***S*-T** aggregates into the most stable supramolecular polymers first at high temperatures and, with the decrease in the temperature, ***S*-B** monomer intercalates into the copolymers, finally showing a predominant alternating fashion in supramolecular copolymers (Scheme 1). This work is a seminal case in which the reactivity ratio $R$ changes from above 1 (1.07 at 110 °C) to below 1 (0.91 at 10 °C) with temperature, making the microstructures of copolymers temperature dependent. The evolution from homopolymers to predominantly alternating copolymers is caused by increased heterointeractions between triazine and benzene cores in ***S*-T** and ***S*-B**, respectively, upon cooling. The temperature-dependent composition change allows reversible removal and addition of supramolecular building blocks in the copolymers and thereby adjusting the polymers' properties, which could potentially be used for novel sensors, temperature-dependent conductors, and optoelectronic devices. The work also shows the general idea that tuning the homointeractions and heterointeractions between monomers makes it possible to have access to supramolecular copolymers with various compositions at various temperatures. Precise control over supramolecular copolymers will eventually


https://doi.org/10.1021/jacs.1c07690
J. Am. Chem. Soc. 2021, 143, 17128−17135

allow for effective tailoring of the functionalities of supramolecular materials.

## ■ ASSOCIATED CONTENT

### Supporting Information

The Supporting Information is available free of charge at https://pubs.acs.org/doi/10.1021/jacs.1c07690.

Experimental procedures and characterization data for all new compounds, photophysical and chemical studies, and details regarding the computational calculations (PDF)

## ■ AUTHOR INFORMATION


### Corresponding Author

**E. W. Meijer** − *Laboratory of Macromolecular and Organic Chemistry and Institute for Complex Molecular Systems (ICMS), Eindhoven University of Technology, 5600 MB Eindhoven, The Netherlands;* orcid.org/0000-0003-4126-7492; Email: E.W.Meijer@tue.nl

### Authors

**Hao Su** − *Laboratory of Macromolecular and Organic Chemistry and Institute for Complex Molecular Systems (ICMS), Eindhoven University of Technology, 5600 MB Eindhoven, The Netherlands*

**Stef A. H. Jansen** − *Laboratory of Macromolecular and Organic Chemistry and Institute for Complex Molecular Systems (ICMS), Eindhoven University of Technology, 5600 MB Eindhoven, The Netherlands;* orcid.org/0000-0002-1505-8462

**Tobias Schnitzer** − *Laboratory of Macromolecular and Organic Chemistry and Institute for Complex Molecular Systems (ICMS), Eindhoven University of Technology, 5600 MB Eindhoven, The Netherlands;* orcid.org/0000-0003-3613-576X

**Elisabeth Weyandt** − *Laboratory of Macromolecular and Organic Chemistry and Institute for Complex Molecular Systems (ICMS), Eindhoven University of Technology, 5600 MB Eindhoven, The Netherlands;* orcid.org/0000-0002-6024-9145

**Andreas T. Rösch** − *Laboratory of Macromolecular and Organic Chemistry and Institute for Complex Molecular Systems (ICMS), Eindhoven University of Technology, 5600 MB Eindhoven, The Netherlands*

**Jie Liu** − *Laboratory of Macromolecular and Organic Chemistry and Institute for Complex Molecular Systems (ICMS), Eindhoven University of Technology, 5600 MB Eindhoven, The Netherlands;* orcid.org/0000-0003-0118-9872

**Ghislaine Vantomme** − *Laboratory of Macromolecular and Organic Chemistry and Institute for Complex Molecular Systems (ICMS), Eindhoven University of Technology, 5600 MB Eindhoven, The Netherlands;* orcid.org/0000-0003-2036-8892

Complete contact information is available at: https://pubs.acs.org/10.1021/jacs.1c07690


### Notes

The authors declare no competing financial interest.

## ■ ACKNOWLEDGMENTS

This project received funding from the Dutch Ministry of Education, Culture and Science (Gravity program 024.001.035), The Netherlands Organization for Scientific Research (NWO-TOP PUNT Grant No. 10018944), and the European Research Council (H2020-EU.1.1., SYNMAT project, ID 788618). T.S. acknowledges the Swiss national science foundation for a Postdoc Mobility fellowship. The authors thank Christiaan Corbet for the help of stopped-flow measurements. The authors also thank Nils C. Jansen for his contribution in synthesizing compounds. Pongphak Chidchob and Anja R. A. Palmans are acknowledged for fruitful discussions.

## ■ REFERENCES


(1) Webber, M. J.; Appel, E. A.; Meijer, E. W.; Langer, R. Supramolecular biomaterials. *Nat. Mater.* **2016**, *15* (1), 13−26.

(2) Su, H.; Wang, F. H.; Wang, Y. Z.; Cheetham, A. G.; Cui, H. G. Macrocyclization of a Class of Camptothecin Analogues into Tubular Supramolecular Polymers. *J. Am. Chem. Soc.* **2019**, *141* (43), 17107−17111.

(3) Cui, H. G.; Webber, M. J.; Stupp, S. I. Self-Assembly of Peptide Amphiphiles: From Molecules to Nanostructures to Biomaterials. *Biopolymers* **2010**, *94* (1), 1−18.

(4) Schenning, A. P. H. J.; Meijer, E. W. Supramolecular electronics; nanowires from self-assembled pi-conjugated systems. *Chem. Commun.* **2005**, *26*, 3245−3258.

(5) Zhang, W.; Jin, W. S.; Fukushima, T.; Saeki, A.; Seki, S.; Aida, T. Supramolecular Linear Heterojunction Composed of Graphite-Like Semiconducting Nanotubular Segments. *Science* **2011**, *334* (6054), 340−343.

(6) Guler, M. O.; Stupp, S. I. A self-assembled nanofiber catalyst for ester hydrolysis. *J. Am. Chem. Soc.* **2007**, *129* (40), 12082−12083.

(7) Neumann, L. N.; Baker, M. B.; Leenders, C. M. A.; Voets, I. K.; Lafleur, R. P. M.; Palmans, A. R. A.; Meijer, E. W. Supramolecular polymers for organocatalysis in water. *Org. Biomol. Chem.* **2015**, *13* (28), 7711−7719.

(8) Zhang, C. Q.; Xue, X. D.; Luo, Q.; Li, Y. W.; Yang, K. N.; Zhuang, X. X.; Jiang, Y. G.; Zhang, J. C.; Liu, J. Q.; Zou, G. Z.; Liang, X. J. Self-Assembled Peptide Nanofibers Designed as Biological Enzymes for Catalyzing Ester Hydrolysis. *ACS Nano* **2014**, *8* (11), 11715−11723.

(9) Adelizzi, B.; Chidchob, P.; Tanaka, N.; Lamers, B. A. G.; Meskers, S. C. J.; Ogi, S.; Palmans, A. R. A.; Yamaguchi, S.; Meijer, E. W. Long-Lived Charge-Transfer State from B-N Frustrated Lewis Pairs Enchained in Supramolecular Copolymers. *J. Am. Chem. Soc.* **2020**, *142* (39), 16681−16689.

(10) Adelizzi, B.; Van Zee, N. J.; de Windt, L. N. J.; Palmans, A. R. A.; Meijer, E. W. Future of Supramolecular Copolymers Unveiled by Reflecting on Covalent Copolymerization. *J. Am. Chem. Soc.* **2019**, *141* (15), 6110−6121.

(11) Onogi, S.; Shigemitsu, H.; Yoshii, T.; Tanida, T.; Ikeda, M.; Kubota, R.; Hamachi, I. In situ real-time imaging of self-sorted supramolecular nanofibres. *Nat. Chem.* **2016**, *8* (8), 743−752.

(12) Draper, E. R.; Eden, E. G. B.; McDonald, T. O.; Adams, D. J. Spatially resolved multicomponent gels. *Nat. Chem.* **2015**, *7* (10), 848−852.

(13) Frisch, H.; Unsleber, J. P.; Ludeker, D.; Peterlechner, M.; Brunklaus, G.; Waller, M.; Besenius, P. pH-Switchable Ampholytic Supramolecular Copolymers. *Angew. Chem., Int. Ed.* **2013**, *52* (38), 10097−10101.

(14) Das, A.; Ghosh, S. Supramolecular Assemblies by Charge-Transfer Interactions between Donor and Acceptor Chromophores. *Angew. Chem., Int. Ed.* **2014**, *53* (8), 2038−2054.

(15) Song, Q. A.; Kerr, A.; Yang, J.; Hall, S. C. L.; Perrier, S. Tubular supramolecular alternating copolymers fabricated by cyclic peptide-polymer conjugates. *Chem. Sci.* **2021**, *12* (26), 9096−9103.

(16) Chakraborty, S.; Kar, H.; Sikder, A.; Ghosh, S. Steric ploy for alternating donor-acceptor co-assembly and cooperative supramolecular polymerization. *Chem. Sci.* **2017**, *8* (2), 1040−1045.
(17) Besenius, P. Controlling supramolecular polymerization through multicomponent self-assembly. *J. Polym. Sci., Part A: Polym. Chem.* **2017**, *55* (1), 34−78.
(18) Sarkar, A.; Sasmal, R.; Empereur-mot, C.; Bochicchio, D.; Kompella, S. V. K.; Sharma, K.; Dhiman, S.; Sundaram, B.; Agasti, S. S.; Pavan, G. M.; George, S. J. Self-Sorted, Random, and Block Supramolecular Copolymers via Sequence Controlled, Multicomponent Self-Assembly. *J. Am. Chem. Soc.* **2020**, *142* (16), 7606−7617.
(19) Adelizzi, B.; Aloi, A.; Markvoort, A. J.; Ten Eikelder, H. M. M.; Voets, I. K.; Palmans, A. R. A.; Meijer, E. W. Supramolecular Block Copolymers under Thermodynamic Control. *J. Am. Chem. Soc.* **2018**, *140* (23), 7168−7175.
(20) Gorl, D.; Zhang, X.; Stepanenko, V.; Würthner, F. Supramolecular block copolymers by kinetically controlled co-self-assembly of planar and core-twisted perylene bisimides. *Nat. Commun.* **2015**, *6*, 7009.
(21) Jung, S. H.; Bochicchio, D.; Pavan, G. M.; Takeuchi, M.; Sugiyasu, K. A Block Supramolecular Polymer and Its Kinetically Enhanced Stability. *J. Am. Chem. Soc.* **2018**, *140* (33), 10570−10577.
(22) Sarkar, A.; Sasmal, R.; Das, A.; Venugopal, A.; Agasti, S.; George, S. J. Tricomponent Supramolecular Multiblock Copolymers with Tunable Composition via Sequential Seeded Growth. *Angew. Chem., Int. Ed.* **2021**, *60* (33), 18209−18216.
(23) Cantekin, S.; de Greef, T. F. A.; Palmans, A. R. A. Benzene-1,3,5-tricarboxamide: a versatile ordering moiety for supramolecular chemistry. *Chem. Soc. Rev.* **2012**, *41* (18), 6125−6137.
(24) Ugozzoli, F.; Massera, C. Intermolecular interactions between benzene and 1,3,5-triazine: a new tool for crystal engineering and molecular recognition. *CrystEngComm* **2005**, *7*, 121−128.
(25) Smulders, M. M. J.; Nieuwenhuizen, M. M. L.; de Greef, T. F. A.; van der Schoot, P.; Schenning, A. P. H. J.; Meijer, E. W. How to Distinguish Isodesmic from Cooperative Supramolecular Polymerisation. *Chem. - Eur. J.* **2010**, *16* (1), 362−367.
(26) Zhao, D. H.; Moore, J. S. Nucleation-elongation: a mechanism for cooperative supramolecular polymerization. *Org. Biomol. Chem.* **2003**, *1* (20), 3471−3491.
(27) Vyas, V. S.; Haase, F.; Stegbauer, L.; Savasci, G.; Podjaski, F.; Ochsenfeld, C.; Lotsch, B. V. A tunable azine covalent organic framework platform for visible light-induced hydrogen generation. *Nat. Commun.* **2015**, *6*, 8508.
(28) Palmans, A. R. A.; Vekemans, J. A. J. M.; Havinga, E. E.; Meijer, E. W. Sergeants-and-soldiers principle in chiral columnar stacks of disc-shaped molecules with C-3 symmetry. *Angew. Chem., Int. Ed. Engl.* **1997**, *36* (23), 2648−2651.
(29) Das, A.; Vantomme, G.; Markvoort, A. J.; ten Eikelder, H. M. M.; Garcia-Iglesias, M.; Palmans, A. R. A.; Meijer, E. W. Supramolecular Copolymers: Structure and Composition Revealed by Theoretical Modeling. *J. Am. Chem. Soc.* **2017**, *139* (20), 7036−7044.
(30) ten Eikelder, H. M. M.; Adelizzi, B.; Palmans, A. R. A.; Markvoort, A. J. Equilibrium Model for Supramolecular Copolymerizations. *J. Phys. Chem. B* **2019**, *123* (30), 6627−6642.


https://doi.org/10.1021/jacs.1c07690
*J. Am. Chem. Soc.* 2021, 143, 17128−17135